Chapter 6 Aeolian Geomorphology and its Simulation–Aeolian Sand Ripples

In desolate deserts, sand particles are arranged by wind into various geomorphologic patterns, like aeolian sand ripples and aeolian sand dunes, according to certain rules. Aeolian landforms exist not only on Earth (see Fig. 6.1) but also on other planets, such as Mars (see Fig. 6.2). Strikingly, the corresponding patterns on different planets and the different patterns on a same planet have a similarity. Therefore, it is meaningful to reveal the dominating mechanism governing the formation, evolution and distribution of aeolian landforms, which is beneficial to the understanding of wind erosion, transportation and deposition of sand (dust) materials. In addition, it is also helpful to the theoretical guidance for the designs of sand-fixing facilities and sand-controlling projects in deserts, for example, the roads and railways passing through deserts are required to avoid the moving route of sand dunes.

Aeolian geomorphology system is a typical complex dynamical system, which presents a complex hierarchical structure. The scales of ripples, dunes and draas are 10^{-2}–10^{-1} m, 10^{-1}–10^{2} m and 10^{2}–10^{3} m respectively. Ripples, as the smallest member of the hierarchy, are frequently observed on sand bed surface and dune surface. Although neither ripples can grow into dunes nor can dunes grow into draas and their formation mechanisms are not the same, all of these three landforms' patterns have an obvious similarity (see Figs. 6.1 and 6.2). Surprisingly, such inerratic and orderly patterns are derived from disorderly moving of sand particles, whose scale is micrometer in magnitude. Besides, there are many interesting phenomena; for example, the self-reparation of ripples on a smoothed surface under wind action, and the critical collapsing or 'avalanche' during sand accumulation. These together make the aeolian geomorphology system be a characteristic example and natural laboratory for non-linear science. More and more scientists in mathematics, physics, mechanics, and other fields have been paying attention to this subject. Till now, aeolian desert geomorphology system has been an important subject of granular material research. The rich spatial-temporal dynamical behaviors involved in the aeolian geomorphology system make it also be a typical example in pattern

X. Zheng, *Mechanics of Wind-blown Sand Movements*, Environmental Science and Engineering,
DOI 10.1007/978-3-540-88254-1_6,

dynamics. Moreover, macro-scale phenomena of aeolian geomorphology system in deserts can give an image comparison explanation to microscopic structures of crystal and many other materials. For example, sand pile models have long been used to study superconductor (Gennes 1966). The formation mechanism of large compound sand dunes will help deepen understanding the process of biological evolution from simplicity to complexity, etc. Altogether, the understanding, recognition and description of aeolian geomorphology system, which mainly include multi-level, transscale, self-organization, self-reparation, critical and non-linear properties

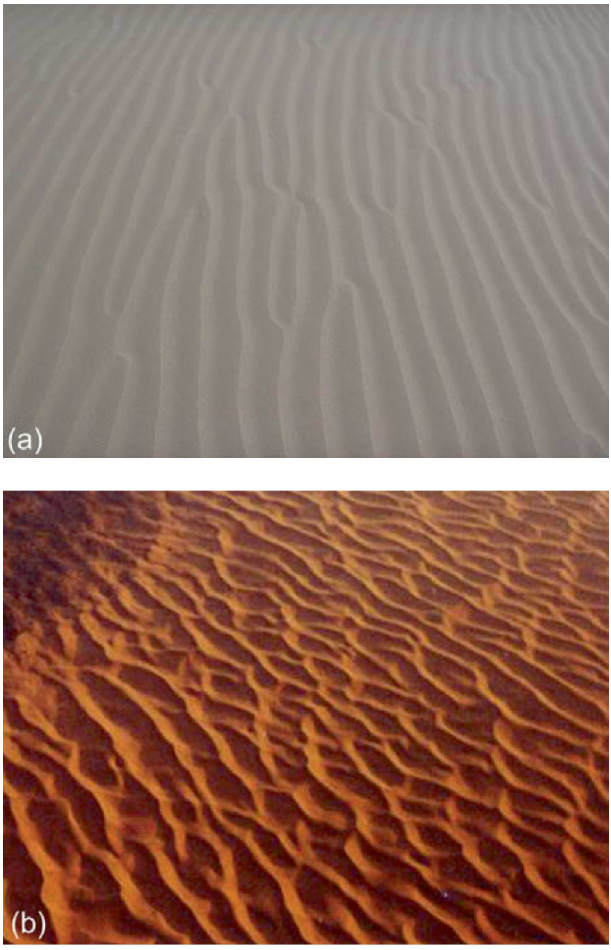

Fig. 6.1. Aeolian landforms on Earth, **(a)** aeolian sand ripples in the Badain Jaran Desert (photo by the author et al.) and **(b)** aeolian sand dunes in the Tengger Desert, China (photo by YQ Ling)

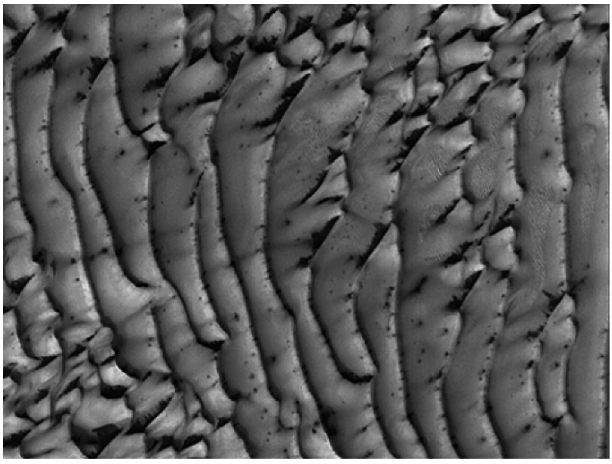

Fig. 6.2. Frost covered sand dunes in the Martian North polar region acquired by Mars Orbiter Camera on 29 August 2005 (Courtesy NASA/JPL-Caltech)

of complex systems, and the development process from disorder to order (Shinbrot and Muzzio 2001) have been fundamental issues in numerous scientific forefronts. It has universality and extreme significance in science (Werner 1999).

This chapter will mainly launch the discussion on aeolian sand ripples. In Sect. 6.1, some field observations and wind tunnel experiments on basic features of aeolian sand ripples and their formation mechanism are introduced. Sects. 6.2 and 6.3 provide two main methods used for simulating the formation and evolution of aeolian sand ripples, namely, the continuous sand ripples model and discrete sand ripples models. Sect. 6.4 devotes to the description of the discrete particle tracing method, a new numerical method proposed by the author et al. to simulate aeolian sand ripples. The results of this method agree with the real formation and development process of aeolian sand ripples not only in quality (in pattern) but also in spatial and temporal scale.

6.1 Observations of Aeolian Sand Ripples

6.1.1 The Basic Characteristics of Aeolian Sand Ripples

Aeolian sand ripples refer to the slight fluctuation on loose sand surface under wind action, which is usually accompanied by the Y-junctions or

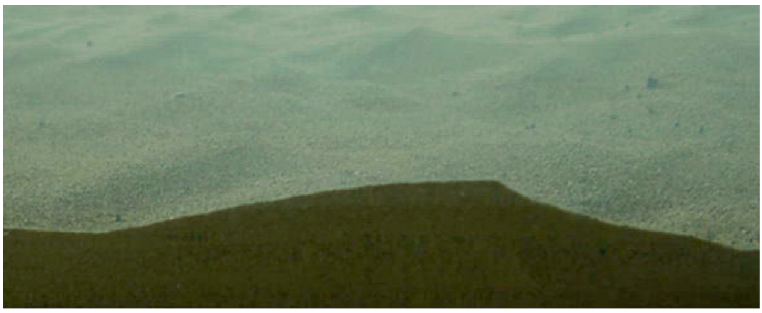

Fig. 6.3. The cross-section profile of a aeolian sand ripple captured in wind tunnel, the axial wind velocity is 12 $m \cdot s^{-1}$, the sand is natural dune sand sampled from the Badain Jaran Desert, China, and the size distribution of sand particles is shown in Fig 4.1 (photo by the author et al. in the multi-function wind tunnel of Lanzhou University)

bifurcations (Fig. 6.1a). The spacing between neighboring crests is approximately uniform, namely the wavelength. Field observations and wind tunnel experiments show that aeolian sand ripples have the following properties.

Asymmetric Shape: The profile of an aeolian sand ripple is obviously asymmetry. From wind tunnel experiments (Here, the sand used in experiment is natural dune sand sampled from the Badain Jaran Desert, China), it can be found that when wind velocity varies from 7 $m \cdot s^{-1}$ to 20 $m \cdot s^{-1}$, the saturated ripple is asymmetric (see Fig. 6.3), with a convex windward (stoss) slope having a angle of 8°–15° and a concave leeward slope. For the leeward slope, the angle in the peak is about 30° which is close to the repose angle of sand, whereas the slope angle at the bottom is a little smaller, which is about 20°. The wavelength λ of a ripple is typically between 7.5–15 cm, and amplitude H is between 0.5–1.0 cm. The ripple index $RI = \lambda / H$ and symmetry index $RSI = i / s$ are usually used to depict the undulation shape characteristic, where i and s are the projected length of windward slope and leeward slope respectively. Our field observations in the Badain Jaran Desert showed that the ripple index lies in a range of $9 \leq RI \leq 22$ and has a linear relationship with the wind velocity. The average index is about 15, which is a little smaller than the ripple index of 18 in the Mojave Desert Kelso Dunes of the United States (Sharp 1963). That may be caused by the difference of wind velocity and size distribution of sand particles.

Wind Velocity Relativity: The results of both wind tunnel experiments and field observations show that the wavelength of an aeolian sand ripple increases with wind velocity. In the developmental stage of an aeolian sand ripple, its amplitude slowly increases with the wind velocity, but

when wind velocity exceeds a certain threshold, which is about 14 $m \cdot s^{-1}$ (the axis wind velocity in wind tunnel), its wavelength decreases with wind velocity and the ripple starts dying out. Similarly, the ripple index increases with the wind velocity. However, the symmetry index has little change with variations of wind velocity (Ling et al. 1998). Generally speaking, under the blowing of high-velocity wind, ripples become straight, ripple index reaches as high as 50–60, and the threshold wind velocity for the disappearance of aeolian sand ripples is about 3–4 times to the threshold wind velocity for the startup of sand particles. In addition, our field observations conducted in the Badain Jaran Desert of China showed that: the ripples in the windward and the leeward slope of dune arms have slightly different disposition. Generally, the ripple index in the windward slope is greater than that in the leeward slope. In the windward slope of a dune, the direction of ripple's crest is normal to the main wind direction and the scales of ripples increase with the height of bed surface. While in the leeward slope of a dune, the direction of ripple's crest is parallel to the main direction extending from the dune crest to the foot of the leeward and their wavelengths and amplitudes first increase and then

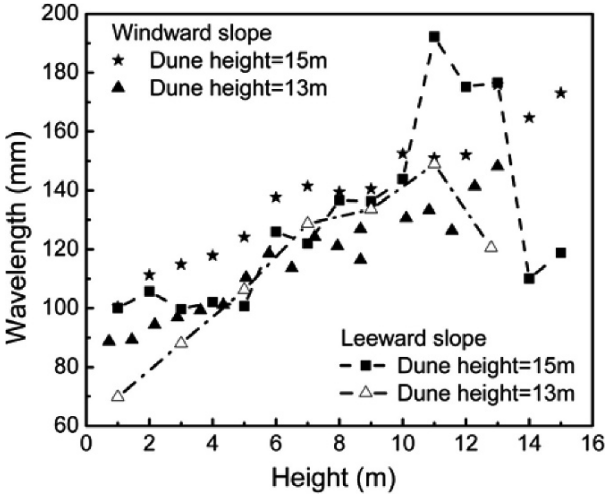

Fig. 6.4. The variations of saturated ripple's wavelength with the surface height; the measurements are conducted at windward and leeward slopes respectively on two sand dunes in the Badain Jaran Desert (by the author et al.); ★ the results measured on the windward slope of a 15 m-high dune, ▲ the results measured on the windward slope of a 13m-high dune, –■– the results measured on the leeward slope of a 15 m-high dune, –△– the results measured on the leeward slope of a 13m-high dune

decrease with the height of bed surface (see Fig. 6.4). For the Y-junctions, the wavelength of upwind junction is less than that of downwind, and their difference first decreases and then increases with the friction wind velocity (see Fig. 6.5).

Particle Diameter Dependence: Both of the wavelengths and the amplitudes of ripples are proportional to the sand diameter. For example, Stone and Summers (1972) suggested that $L = 63.8D_s^{-0.75}$; here, D_s (mm) is the average sand diameter in the crest of ripples. Usually, aeolian sand ripples present a stratigraphic structure, that is, the coarsest material collects at the crest, and the finest in the trough. This characteristic distinguishes without exception the ripples from the dunes, wherein the reverse is invariably the case (Bagnold 1941). Besides, sand gradation is also a key factor influencing the height and shape of the ripple. For 'uniform' sands, the height of an aeolian sand ripple is relatively low, and the ripple index generally follows $RI < 30$ (Bagnold 1941). However, the ripple with broad size range and poor size separation has a ripple index reaching as low as 15, even about 10. This is because the coarse sand particles are more difficult to be transported under the wind action, and thus gather at the crest of ripple.

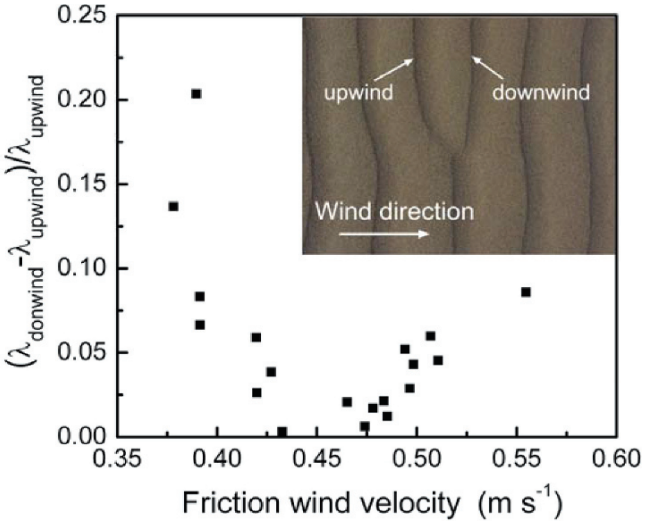

Fig. 6.5. The difference between the downwind wavelength ($\lambda_{downwind}$) and the upwind wavelength (λ_{upwind}) of Y-junctions for different friction wind velocities. ■ – measured data in the Badain Jaran Desert, the embedded picture is a photo of a Y-junction in the field (by the author et al.)

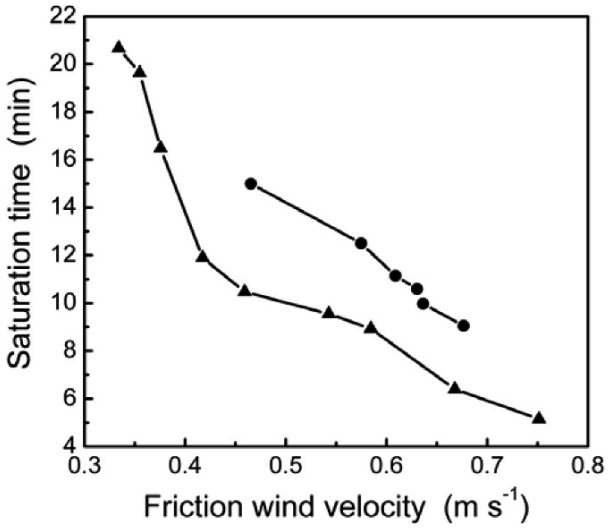

Fig. 6.6. The relation between the saturation time of aeolian sand ripples and friction wind velocity; –●– measured results in the Badain Jaran Desert; –▲– measured results in the multi-function environmental wind tunnel of Lanzhou University (by the author et al.)

Development Stage: Wind tunnel experiments (Andreotti et al. 2006) and our field observations showed that the formation of aeolian sand ripples can be divided into three stages: Initially, the flat sand bed deforms and tiny structures appear, then the tiny structures start merging so that the pattern exhibits coarsening, and finally the pattern tends to be saturated. After saturation, the ripples maintain their forms and sizes to move along the wind direction with velocities proportional to the friction wind velocity. Our experiments also find that the duration of ripples developing from initial unsaturation to saturation decreases with the increase of the friction wind velocity (see Fig. 6.6), and the saturation time in the field is longer than wind tunnel which probably results from the intermittency of natural wind. Besides, aeolian sand ripples are capable of self-reparation (Sharp 1963), that is, when destroyed, the ripples will reappear under wind action, and these ripples will connect with other neighboring ripples gradually, and ultimately eliminate the traces of breakage.

6.1.2 The Formation Mechanism of Aeolian Sand Ripples

There have been many hypotheses proposed to explain the formation mechanism of aeolian sand ripples, including the separation hypothesis, the

wave hypothesis and the impact hypothesis. The separation hypothesis (Энаменский 1960) considered the formation of aeolian sand ripples as a result of the separation of moving sand particles of different size, which led the coarse sand particles accumulating on the crest and fine sand on the trough. The wave hypothesis (Cooke et al. 1993) suggested that ripples are formed by the regular small-scale vortex structure near the bed surface generated by the unstable airflow in the atmospheric boundary layer. Another interpretation of wave hypothesis (Kennedy 1969) deemed the Helmholtz's wave as a main reason of aeolian sand ripples' formation. The Helmholtz's wave appears at the interface between two different density flows - sand particle flow and air flow. Now more generally accepted hypothesis is the impact hypothesis proposed by Bagnold (1941). The impact hypothesis thinks that the formation of aeolian sand ripples is mainly due to the collision between saltating sand particles and bed surface. In other words, due to the existence of a number of tiny unevennesses of sand surface, the intensity of bombardment on windward slope is higher than that on leeward slope, which results in the original hollow getting bigger. And since the bombardment is more intense on the windward slope than it is on the level surface downwind, the particles that have been excavated from the hollow will accumulate at the junction of windward slope and downwind surface, because they are not being removed downwind as quickly as they are coming. As the accumulation at the junction rises, it forms a second lee slope, and here the particle movement is again feeble. This in turn causes the surface at the foot of the second lee slope to be depleted of particles, because they are being removed faster than they can now move down the second leeward slope by a more intense bombardment. Therefore, a second hollow is formed, and so on. From the above, it appears that a flat sand surface must be unstable, because any occasional deformation tends to become accentuated by the local sand-removing action of the saltation.

It is a difficult task to investigate the validity of the above hypotheses from the perspective of field observations and wind tunnel experiments, because the temporal and spatial scale involved in the formation and evolution of aeolian sand ripples are too small, the reliability of direct observation to a large extent depends on the resolution and accuracy of observation methods and equipments. Therefore, theoretical modeling and computer simulation may serve as important supplements to reveal the process, the mechanism and the laws of the formation and development of aeolian sand ripples.

6.2 Continuous Models for Aeolian Sand Ripples

In continuous models, the bed elevation $z(x, t)$ is treated as an undetermined function of the horizontal coordinate x paralleling to the wind direction and time t. Through solving the differential equations based on corresponding initial and boundary conditions, we can determine the bed elevation and its rate of change. Here, we briefly introduce two types of continuous model: the Anderson's continuous model (1987) which is based on saltating movement of sand particles, and the granular surface flow model based on hydrodynamics.

6.2.1 The Anderson's Continuous Model

A high-energy impact characteristically gives rise to several low-energy ejection particles which leap once near the surface with a distance smaller than saltation length but longer than creeping length. This movement of sand particles is so-called reptation. Anderson (1987) deemed that the instability of bed surface is mainly caused by the reptating sand, but not the saltating sand. Therefore, the rate of change of bed elevation is a function of the divergence of reptating sand flux. We denote the mass of sand particle by m_s,, the reptation length by l_{rep}, the number of reptating particles per unit area per unit time by N_{ej} which is related to the number of saltating particles N_s arriving at a flat horizontal bed per unit area per unit time and the number of particles n_0 ejected per impact, the incident angle of the impacting particles by θ and the angle the bed makes with the horizontal by α, then N_{ej} can be written as:

$$N_{ej} = N_0 n_0 \left(1 + \frac{\tan\theta}{\tan\alpha}\right)\cos\theta . \tag{6.1}$$

In this way, the flux of reptating particles $Q_{rep}(x)$ at x can be expressed as

$$Q_{rep}(x) = m_s \int_{x-l_{rep}}^{x} N_{ej}(x')dx' = m_s \int_{x-l_{rep}}^{x} N_s(x')n_0(x')\left(1+\frac{\tan\alpha}{\tan\theta}\right)\cos\alpha dx' \tag{6.2}$$

When the wind-blown sand flow achieves steady-state, the flux of reptating particles should be subject to the forms of mass conservation equations. Taking into account the bed slope $\tan\alpha = \partial z / \partial x$, accordingly, partial differential equations for the rate of change of bed elevation are:

$$\frac{\partial z}{\partial t}=\frac{m_s n_0 N_s}{\rho_b}\left(1+\frac{\partial z}{\partial x}\cot\theta\right)\left[1+\left(\frac{\partial z}{\partial x}\right)^2\right]^{-\frac{1}{2}} \qquad x\in\left[x-l_{rep},x\right] \tag{6.3a}$$

$$t=0: \quad z_{ini}=z_0 e^{ikx} \tag{6.3b}$$

Here, $\rho_b=(1-\eta)\rho_s$ is the bulk density of the sediment in the bed, ρ_s is the particle density, and η is the porosity of the bed. A translating sinusoidal perturbation z_{ini} on a flat granular bed is assumed, in which z_0 is the initial amplitude of the bedform (half of the height from the trough to the crest of form), k is the wave number of ripples, i is the imaginary unit and the sand flux passing through arbitrary cross-section per unit time is the total particles ejected from $x-l_{rep}$ to x, therefore, the value of integral upper limit and lower limit of bed elevation are $x-l_{rep}$ and x respectively.

According to the Anderson's continuous model (1987), we can obtain the laws of the translation velocity c_i and the growth rate c_r of ripple amplitude changing with the ratio between wavelength λ and the reptation length l_{rep} (see Fig. 6.7). From Fig. 6.7, it can be found that both the translation velocity and the growth rate first increase and then decrease with λ/l_{rep} for (I) uniform reptation length, (II) exponential distribution of reptation lengths and (III) Gamma distribution of reptation lengths, that is, with the increase of ripple wavelength, the growth rate of ripple amplitude changes quickely and then slowly reaching its maximum value at the peak point. However, the peak point of the growth rate of ripple amplitude is different. For case (I), the peak points locate at $\lambda/l_{rep}=4/(2n-1)$, ($n=1$, 2, …); For (II) and (III), they have only one location, that is $\lambda/\overline{l}_{rep}\approx 6$. In addition, for case (I) and (II), the translation velocity decreases with the wavelength, but for case (III), with wavelength increasing, the translation velocity firstly increases and then decreases, reaching its maximum at $\lambda/\overline{l}_{rep}\approx 2$.

Although Anderson's continuous model (1987) has considered the erosion process on bed surface through connecting the change of bed surface with erosion rate, but it did not consider the deposition process of wind-blown sand flow, which is significant to the formation of aeolian sand ripples. In addition, since the motion of sand particles in this model are considered as 'uniform reptation', namely the diameter of saltating sand D_s, the impact angle θ, the reptation length l_{rep}, the number of saltating particles N_s arriving at a flat horizontal bed per unit time per unit area, and the number of ejected particles per impact n_0 are all taken identically, so the simulated aeolian sand ripples are symmetric, and do not have the same

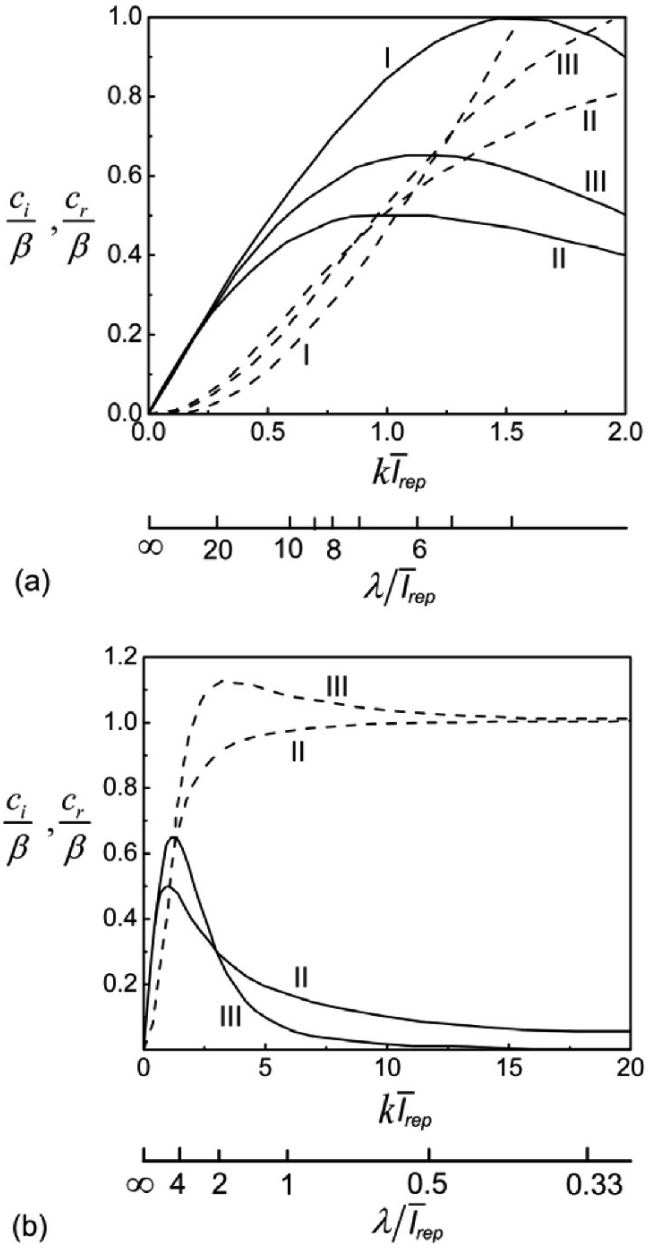

Fig. 6.7. The variations of the growth rate c_r and the translation velocity c_i with reptation length l_{rep} for (I) uniform reptation length, (II) exponential distribution of reptation lengths and (III) Gamma distribution of reptation lengths where $\lambda = 2\pi / k$, $\beta = (mn_0N_0\cot\alpha) / \rho$ (redrawn from Anderson 1987).

characteristic of leeward slope as actual situation. Though the translation velocity c_i and the growth rate c_r of ripple amplitude changing with the ratio between the wavelength and the reptation length were discussed in this model, but the fact that the wavelength of aeolian sand ripples are varying during the formation of aeolian sand ripples was neglected.

6.2.2 The Granular Surface Flow Model

In recent years, the granular surface flow model which is inspired from the viewpoint of phase transition in the hydrodynamic theory has been developed to study the aeolian sand ripples. It was originally employed to investigate the subaqueous ripple (Cornish and Jeffreys 1934), and then was adapted to study the formation of aeolian sand ripples by Bouchaud and his coworkers (Bouchaud et al. 1994). This model is a kind of continuous description where dynamics of the two pertinent particle layers, that is the surface flowing layer and the static layer, are considered separately. The former (including reptation layer and saltation layer) is characterized as a flow phase with the average velocity $\overline{V}_f$ and moving particles density $N_u(x, t)$, while the latter is considered as a solid phase with the height $z(x, t)$. So the formation process of aeolian sand ripples can be regard as a phase transition process caused by mass exchange between the surface flowing layer and the static layer. Assume that the rate of change of bed elevation in solid phase is $\partial z(x,t)/\partial t = \Gamma$, due to the reason that the height of solid phase is a result of the deposition rate Γ_{dep} and the ejection rate Γ_{ej}, which follows: $\Gamma = \Gamma_{dep} - \Gamma_{ej}$, the rate of change of thickness of the surface flowing layer can be expressed as:

$$\frac{\partial N_u}{\partial t} = \overline{V}_f \frac{\partial N_u}{\partial x} - \Gamma(x,t) \tag{6.4}$$

Many analytical models of aeolian sand ripples have been derived based on different descriptions of Γ_{ej} and Γ_{dep}. For example, Prigozhin (1999) deemed that: the ejection rate Γ_{ej} is related to the impact of saltating sand, while the deposition rate Γ_{dep} is related to the accumulation of reptating sand particles which are determined by bed slope and the number of sand particles in the surface flowing layer. According to the way of sand motion, the deposition rate is assumed to be proportional to the number R of reptating particles, that is $\Gamma_{dep}=N_u/t_{dep}$, where, where t_{dep} represents the typical time during which the reptating particles are moving before being incorporated to the sand bed. Through introducing the erosion rate c_1 of flat bed surface determined by the intensity of saltating sand, and the recip-

rocal of reptating time c_2 respectively, we can consider the influence of the impact angle θ of saltating sand, bed slope α and repose angle α_r to the exchange rate between the moving particles and the particles at rest, which can be expressed as:

$$\frac{\partial z}{\partial t} = \Gamma_{dep} - \Gamma_{ej} = c_2 N_u \left(\frac{1 - |\nabla z|^2}{\tan^2 \alpha_r} \right) - \frac{c_1}{\sin\theta} \sin(\theta + \alpha) \tag{6.5}$$

Combining Eqs. 6.5 and 6.3b, it establishes a fixed solution problem of the height $z(x, t)$. Different from the Anderson's continuous model (1987) (Eq. 6.3), Prigozhin (1999) takes into account the rolling and avalanching movement of particles under the influence of the gravity in leeward, the shadowing effect of leeward slope (see Fig. 6.8) and the influence of deposition rate Γ_{dep} to the variation of bed surface. It successfully reproduced the asymmetrical ripple pattern, and forecasted the variation of scale during the evolution process and the typical ripple interaction (see Fig. 6.9). However, it still exists deficiency, that is, the slope angle, scale and development process of simulated ripples by Prigozhin (1991) are inconsistent with the actual states. For example, the wavelengths of natural aeolian sand ripples are generally 7–15 cm, but the simulated results showed that the wavelength can reach up to 33 cm which is bigger than the scale of actual sand ripples. This is mainly because Prigozhin's model (1999) neglected the influence of bed surface curvature to the ejection rate Γ_{ej} and deposition rate Γ_{dep}. In addition, the erosion rate c_1 and the reciprocal of reptating time c_2 are artificially set as constants in this model. However, in fact, it should be related with wind velocity, surface configuration and sand diameter at the eroded position.

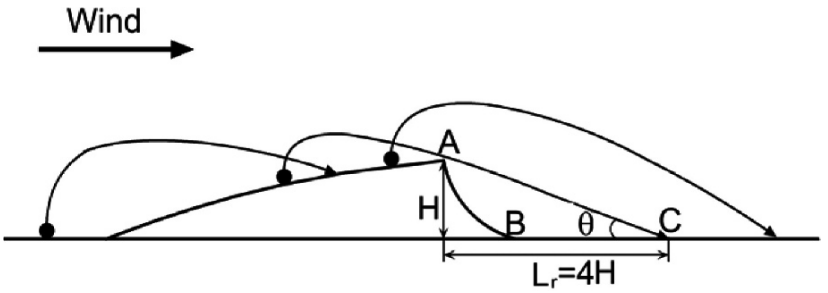

Fig. 6.8. The schematic illustration of the shadowing effect of leeward slope. ● represents the saltating sand; θ is impact angle of saltating sand. Due to the shadowing effect of leeward slope, the area *ABC* is protected from the impact of saltating sand particles, which is so-called the protection zone, *H* is the height of the aeolian sand ripple, L_r is the length of the protection zone

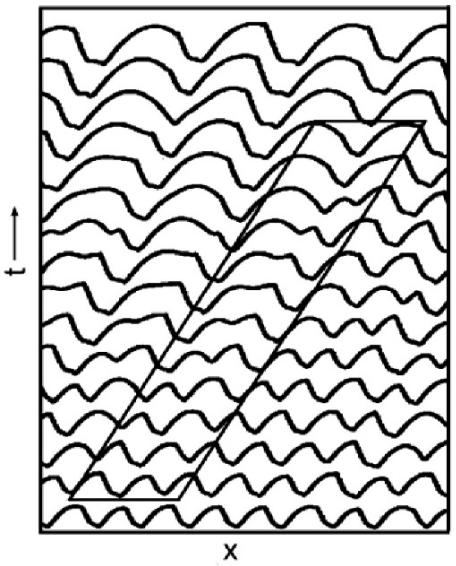

Fig. 6.9. The evolution of aeolian sand ripples predicted by Prigozhin's model (from Prigozhin 1999)

As an improvement of Prigozhin's model (Prigozhin 1999), Valance and Rioual (1999) deemed the ejection rate Γ_{ej} as a result of the impact of saltating particles and the direct entrainment of wind force, that is, $\Gamma_{ej} = \Gamma_{ej}^{imp} + \Gamma_{ej}^{wind}$. This model adopted the expression of the number of ejected particles per unit time per unit area from the surface given by Anderson (1987), and took into account the influence of the bed curvature: $k=(\partial^2 z/\partial x^2)/[1+(\partial z/\partial x)^2]^{3/2}$ (Csahók et al. 2000). The ejection rate in this model therefore can be written as:

$$\Gamma_{ej} = D_s^3 n_0 N_s \left(1 - c_s \frac{\dfrac{\partial^2 z}{\partial x^2}}{\left[1+\left(\dfrac{\partial z}{\partial x}\right)^2\right]^{\frac{3}{2}}} \right) \left(1+\frac{\partial z}{\partial x}\cot\theta\right)\left[1+\left(\frac{\partial z}{\partial x}\right)^2\right]^{-\frac{1}{2}} - \beta_2 \frac{\partial^2 z}{\partial x^2} \tag{6.6}$$

where, β_2 represents the relation between the ejection rate and the bed curvature which can be determined by experiment, and c_s is a constant. The deposition rate Γ_{dep} is assumed to be affected by the bed curvature and slope, that is:

$$\Gamma_{dep} = N_u \gamma_0 \left(1 \pm \gamma_1 \frac{\partial z}{\partial x} + \gamma_2 \frac{\partial^2 z}{\partial x^2} \right) \tag{6.7}$$

where γ_0 corresponds to the reciprocal of typical lifetime of a reptating particle on a flat surface; γ_1 describes the influence of stoss slope gradient, if the wind drag is negligible near the surface, the deposition process will be enhanced on the stoss slope (positive in front of γ_1). But if the wind drag near the bed surface is significant to be considered, the deposition process will be weakened on the stoss slope (negative sign in front of γ_1); γ_2 describes the curvature effect, namely, the bigger the slope curvature and the neighboring slope gradient, the shorter the repating time, and the bigger the deposition probability will be (Hoyle and Mehta 1999).

Substituting the ejection rate Γ_{ej} (i.e. Eq. 6.6) and deposition rate Γ_{dep} (i.e. Eq. 6.7) into $\partial z(x,t)/\partial t = \Gamma_{ej} + \Gamma_{dep}$, it comes into being a fixed solution problem of height $z(x, t)$ for the initial condition (i.e. Eq. 6.3b), which is known as the Valance and Rioual's model (1999).. It can predict the development process and the merger behavior of small ripples. Since the influences of the bed curvature to the deposition rate Γ_{dep} and ejection rate Γ_{ej} are involved during the evolution of aeolian sand ripples, the resulting windward and leeward slope are close to the actual ripples. However, it occurs only when the reptation length l_{rep} is large enough. For the case l_{rep} is small, the windward slope and leeward slope angles do not match, such as the slope angles of windward and leeward will be bigger than the actual values, and there does not exist a saturated status too. It's probably because that the model does not consider the influence of wind velocity, particle diameter and the bed topography to the number of saltating particles hitting a flat surface per unit time and unit surface N_s, the number of ejected particles per impact n_0 and the typical time of reptating particles in air γ_0^{-1}. Besides, some parameters such as β_2, γ_1 and γ_2 must be given in the application of Valance and Rioual's model (1999). to the simulation of aeolian sand ripples, which also makes it difficult to predict the formation and evolution of natural aeolian sand ripples in quantity.

In summary, in the continuous model, an artificially initial bed such as a sinusoid curve is needed, and it can not reflect the influence of wind velocity, diameter and bed topography to the main physical quantities of windblown sand movement, such as the reptation length l_{rep}, the number of saltating particles N_s impacting on a flat surface per unit time and unit surface, the number of ejected particles per impact n_0 and the typical time of reptating particles in air γ_0^{-1}, as well as some parameters such as β_2, γ_1 and γ_2 which are difficult to be determined. Therefore, these models can to some extent reproduce asymmetrical ripples and their growth processes

and interactions. However, the scales of simulated ripples with this class of models do not agree very well with the actual ripples, and the saturation characteristic can not be predicted. These problems cause their simulation results can not connect with wind velocity and diameter of sand particle. Moreover, because of avoiding the discrete character of sand motion, the simulation results can not predict the size segregation of aeolian sand ripples.

6.3 Discrete Models for Aeolian Sand Ripples

In this section, we will introduce briefly three typical discrete models to simulate aeolian sand ripples, they are the Anderson-Bunas model (Anderson and Bunas 1993) based on Cellular Automata method, the Landry-Werner model (Landry and Werner 1994) based on discrete element method and the Nishimori-Ouchi model (Nishimori and Ouchi 1993) based on Coupled mapping lattice method respectively. In the next section, we will present another discrete model proposed by the author et al. recently, that is, the discrete particle tracing method (Zheng et al. 2008) which reflects the entire formation process and the main features of aeolian sand ripples more objectively.

Anderson (1987) addressed that, during the formation of aeolian sand ripples, the 'surface particles' move mainly in the form of reptation, including the ejection, transportation and deposition of reptating sand. The difference among the Anderson-Bunas model (1993), the Landry-Werner model (1994) and the Nishimori-Ouchi model (1993) lies in the treatment of these three key processes; in other words, the artificial rules governing the three processes are distinct.

6.3.1 Cellular Automata Model (Anderson-Bunas Discrete Model)

Cellular automata model is a class of spatially (bed length) and temporally discrete mathematical model characterized by local interaction and synchronous dynamical evolution. The state variables of interest (such as: bed height) at any position in any time can be determined through the state variables of the current and other positions in the previous time. Taking Anderson-Bonas discrete model (Anderson and Bunas 1993) they investigated the formation and evolution of aeolian sand ripples with a two-particle-size cellular automation, the simulation procedures are simplified as follows:

Step 1: Bed surface establishment: Since the Cellular automata model is based on the discrete of the space and the state variables, the model divides the sand bed into a certain number of units along horizontal and vertical direction. For example, the bed was initially 1,250 particles wide and 100 particles deep (Anderson and Bunas 1993) where the lengths and heights of units are both taken as the maximum sand diameter, such as 0.32 mm, that means each cell includes only one sand particle. In the model, the particle size is randomly assigned, with a fine (0.23 mm)/coarse (0.32 mm) ratio of 2:1.

Step 2: Determining the impact velocity of saltating sand and the ejection velocity of reptating sand. After establishing the bed, it requires to select the velocity of impact sand particle on any position of bed surface, and determine the number and velocities of sand particles ejected from impacted position according to certain rules. For example, in Anderson-Bunas discrete model, saltating particles are fired at the bed one by one, the particles that strike the bed have an identical size distribution; impact angle θ and impact velocity V_{im} are randomly selected from a Gaussian distribution with mean value 11°, variance 2° and an exponential distribution $f(V_{im}) = (1/u_*)\exp(-V_{im}/u_*)$, respectively. The mean number of ejecta N_{ej} and the ejection speed V_e can be determined by the soft sphere collision model (in Sect. 3.3.2 and Fig. 6.10). It is worth mentioning that in this model the time of a single impact of sand particle is considered as a computation step, and when the number of computation step is equal to the number of units in the bed surface, then one operation step completes. This kind of stipulation was also introduced into the discrete element method which will be introduced in the following.

Step 3: Stipulating the transportation and deposition of reptating sand. For a given wind velocity, the N_{ej} ejected sand particles, with the ejected velocities V_e are compelled to transportation l_r along wind direction and then deposit. In this model, the transportation distance l_r was calculated by trajectory equation of saltating sand, that is, the saltating length along flat bed surface when wind velocity and diameter is given.

Step 4: Stipulating the number of operation steps. If the current number of operation steps is less than the stipulated number (for example in Anderson and Bunas (1993), the operation steps were 5 million, 10 million and 20 million respectively), then return to the step 2 and carry on the next operation step computation, and the new resulting bed surface is used as the initial bed surface for the next operation step, until the number of operation steps is equal to the stipulated number.

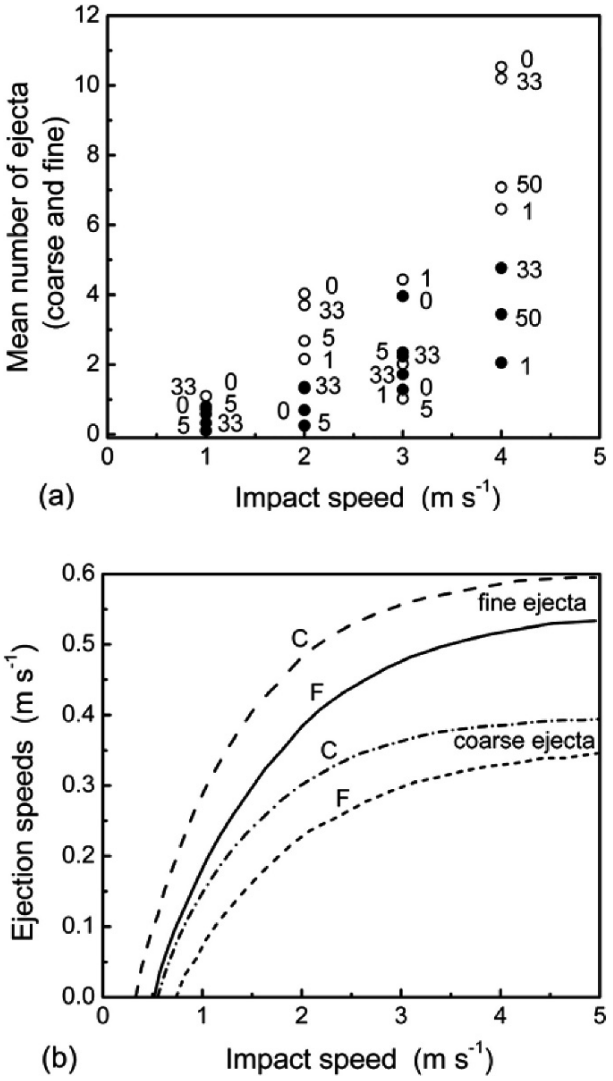

Fig. 6.10. Number of ejected particles and ejection speed per impact as a function of impact speed **(a)** ○ coarse impactor; ● fine impactor **(b)** C and F respectively correspond to the coarse and fine impactor (redrawn from Anderson and Bunas 1993)

The pattern of ripples reproduced by Anderson-Bunas model (1993) is shown in Fig. 6.11. From Fig. 6.11 we can find that the ripples are asymmetric which display convex stoss slopes and concave lee slopes as natural ripples do. Besides, the ripples display strong segregation of particles, that is coarse particles are on the ripple crests, and fine particles are on the

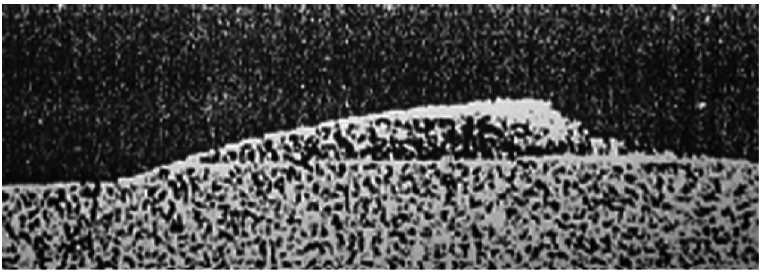

Fig. 6.11. The simulated aeolian sand ripple's shape by cellular automata model (from Anderson and Bunas 1993)

trough of the ripple. However, In Anderson-Bunas model (1993), after each collision the ejected sands lift off from the same position with the same ejected speed, which is contradictory with the actual particle-bed collision process. Moreover, the variation of local topography, such as the salient of bed surface during the formation of aeolian sand ripples can prevent the sand particles to travel l_r which therefore should be treated specifically. In addition, when the reptating sand particles return back to the bed after hopping, the energy is not zero, so they will be rolling a certain distance along sand bed (namely, surface creep); such process has not been considered in this model. More important thing is that although the operation step in this model was called 'time step' (Baas and Nield 2007), in fact, it only represents the completion of one cycle operation. Such kind of 'time step' is very difficult to correspond with actual time, which thus limits the model to reflect the real time scale of the formation and evolution of aeolian sand ripples, especially to reproduce and describe the saturation process of aeolian sand ripples.

6.3.2 Discrete Element Model (Landry-Werner Model)

The Landry-Werner Model (1994) is a kind of three-dimensional Discrete Element Model (DEM) for aeolian sand ripples, where the ejection, transportation and deposition of bed surface sand are parameterized. In the following part, we will take the Landry-Werner model (1994) as an example to introduce its main simulation steps.

Step 1: Generating the bed surface. The establishment of Landry-Werner model (1994) is based on the tracking of the sand motion in system. The bed particles are taken to be a single size (0.25 mm) and are constrained to lie on a hexagonally close packed lattice (Fig. 6.12). The size of bed surface is about 25 × 21 cm, and the bed is initially assumed as a mot-

tled appearance and is characterized by roughly coherent, organized sand piles approximately 2–3 of particle diameters in height.

Step 2: Regulating the transportation distance of reptating sand. Chosing a sand particle from bed surface randomly and making the sand move a distance of l_r along the wind direction. The transportation distance l_r can be determined as follows: first, calculating the average ejected speed base on the soft sphere collision model (in Sect. 3.3.2) on different slope, then determining the saltating distance along the flat bed surface according to the

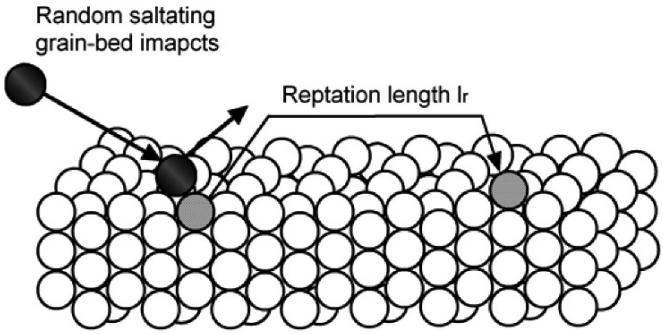

Fig. 6.12. The package of sand particles (redrawn from Landry and Werner 1994)

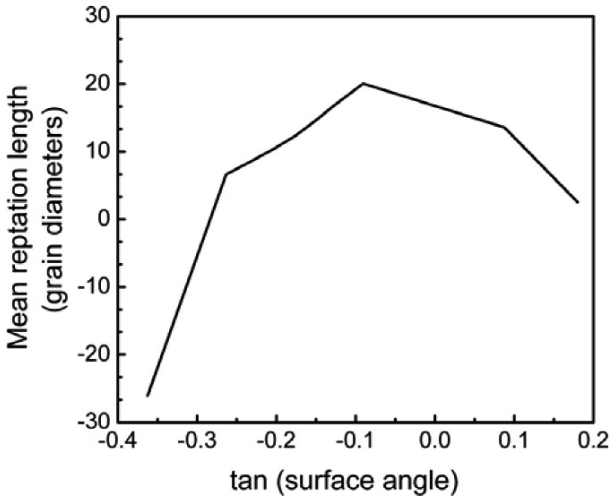

Fig. 6.13. The influence of surface gradient to trajectory length of reptation sand (from Landry and Werner 1994)

trajectory equation of saltating sand (in Sect. 5.), so as to determine the tansport distance of sand in different gradient cases (see Fig. 6.13) ('gradient' algorithm).

Step 3: Regulating the transportation and deposition of reptating sand. The reptating particle is transported a specified number of particle diameters l_r downwind irrespective of the variations of surface gradient during its

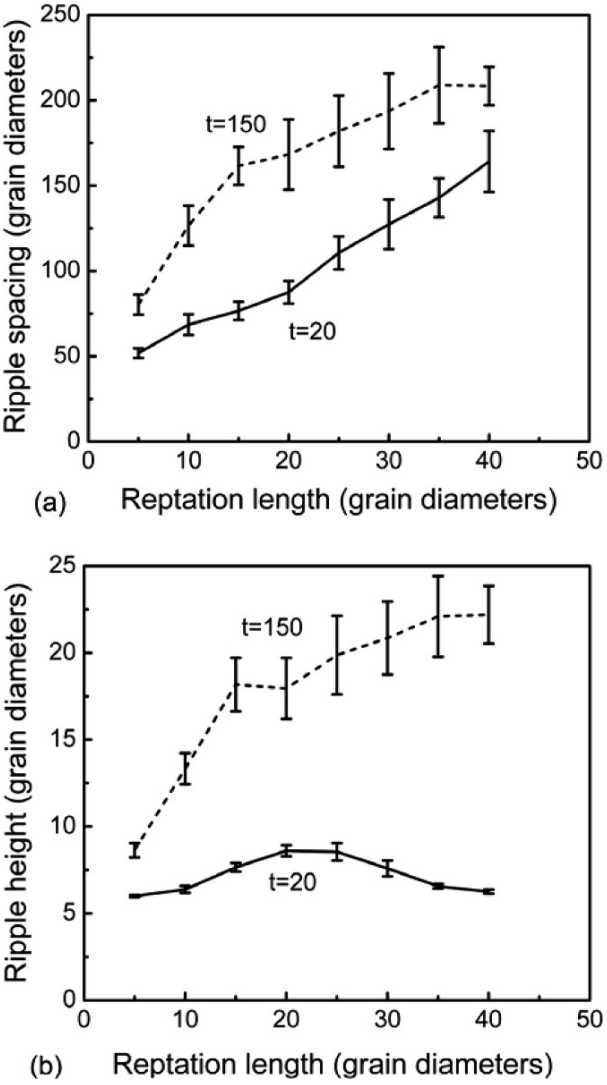

Fig. 6.14. The influence of reptation length to the scale of an aeolian sand ripple, **(a)** ripple spacing and **(b)** ripple length (from Landry and Werner 1994)

movement, and then back to the surface (‘straight ahead’ algorithm). A target particle is given 5 units of pseudo-momentum when it is dropped to the sand bed. Each time the particle moves one particle diameter upslope, it loses 2 units of pseudo-momentum, each time it moves downslope, it gains 1 unit of pseudo-momentum, and each time it moves one lattice spacing without gaining or losing elevation, it loses 1 unit of pseudo-momentum. The sand movement stops until the pseudo-momentum is zero (‘rolling’ algorithm).

Step 4: Stipulating the number of operation steps. One operation step is finished till all the reptating and the creeping sand particles stay on the bed surface. If the current number of operation steps is less than the stipulating number of operation steps, then return to the step 2, and carry on the next operation step computation. The resulting bed surface is used as the initial bed surface for the next operation step, until the number of operation step is equal to the stipulation.

The Landry-Werner model (1994) can also obtain the asymmetrical shape of sand ripple. Compared with the cellular automaton model, its advantage lies in investigating the influence of the reptation length to the scale of an aeolian sand ripple, namely, with the increase of reptation length the scale of the aeolian sand ripple increases (including height and spacing, see Fig. 6.14). Moreover, this model is a three dimensional model which therefore can reproduce the Y-junctions.

However, in Landry-Werner model (1994), the wavelength of the simulated aeolian sand ripples range from 1.25 cm to 5 cm, which is lower than actual values from 7 cm to 15 cm. This is possibly because it doesn’t involve the actual particle-bed collision process and the surface creeping of sand particles. Similar with the Cellular Automaton Model (Anderson-Bunas discrete model (1993)), the operation step in Landry-Werner model (1994) can not correspond with the actual time, so the simulation result can not reflect the actual evolution of aeolian sand ripples, especially the development process from unsaturation to saturation.

6.3.3 Coupled Mapping Lattice Model (Nishimori-Ouchi Model)

The Coupled Mapping Lattice Model is a discrete model in space (the length and width of bed surface) and time with a continuous field variable representing the averaged bed height at each site. The simulation was realized by setting the exchange rule of sand flux, namely by setting the sand exchange between different positions to describe the sand movement. The model assumes that there are two types of sand movement, reptation and

creeping (due to the gravity action). Taking the Nishimori-Ouchi Model (1993) for example, the simulation is performed as follow:

Step 1: Generating the bed surface. This kind of model was established by discretizing the space variable. The bed surface was divided along horizontal and lateral direction into 100×100 cells, the length and width of each cell are larger than sand diameter; a continuous field variable was introduced to describe the bed height, that is, to describe the variations of the number of sand particles in each cell. The height of each cell was randomly determined satisfying the average height is zero.

Step 2: Regulating the transported sand amount and distance. In each operation step, the sand will lift off from all cells, and transport a certain distance L. In this process, the transported sand amount Q_L is identically taken as constant in each cell, the transportation distance can be determined by $L = L_0 + bh_n(x, z)$, here, L_0 is basic reptation length, which is change from 2.5 to 6.5, b is constant, $h_n(x, z)$ is the bed surface in the cell.

Step 3: Regulating rules of creep dynamics. The model determines the exchange sand amount between neighboring cells according to height difference between the nearest and the next nearest cells, so as to keep the height difference satisfying the specified value determined by the repose angle of sand particle.

Step 4: Regulating the number of the operation steps. When all sands stay on the bed surface, one operation step calculation is finished. If the operation step is less than the required operation step, then return to the step 2, and carry on the next operation step computation based on the new bed surface, until it reaches the stipulated number.

Comparing the two models introduced above, the Nishimori-Ouchi model (1993) can also present the asymmetrical shape of aeolian sand ripples and their growth processes. Moreover, it can also obtain the Y-junctions and self-reparation behavior of aeolian sand ripples in three-dimensional space. The merit of this kind of model is few computation cells are required in the simulation, and it has no need to trace every sand particle, but only need to trace the spatial positions, which together to some extent reduce the computation complexity. Besides, the influence of L_0 to the scale of aeolian sand ripples can also be investigated (see Fig. 6.15).

However, in this model, the height of the bed surface is not discretized, which results in the simulation not being able to reflect the stratigraphic structure of aeolian sand ripples. At the same time, it is worth pointing out that each operation step in this model represents the time required for the fulfillment of all erosion and deposition processes on the bed. Due to the transportation distance and creep rule are artificially regulated, this model

can not reflect the corresponding relationships with the real time. In addition, the erosion and deposition of sand particles are not identical everywhere during the formation of aeolian sand ripples.

In summary, although the three kinds of discrete models mentioned above can to some extent reflect the splash, transportation and deposition of reptating sands during the formation of aeolian sand ripples, but they generally resort to some artificial rules or hypotheses which to a large extent limit the accuracy and validity of their simulations. The rules in above

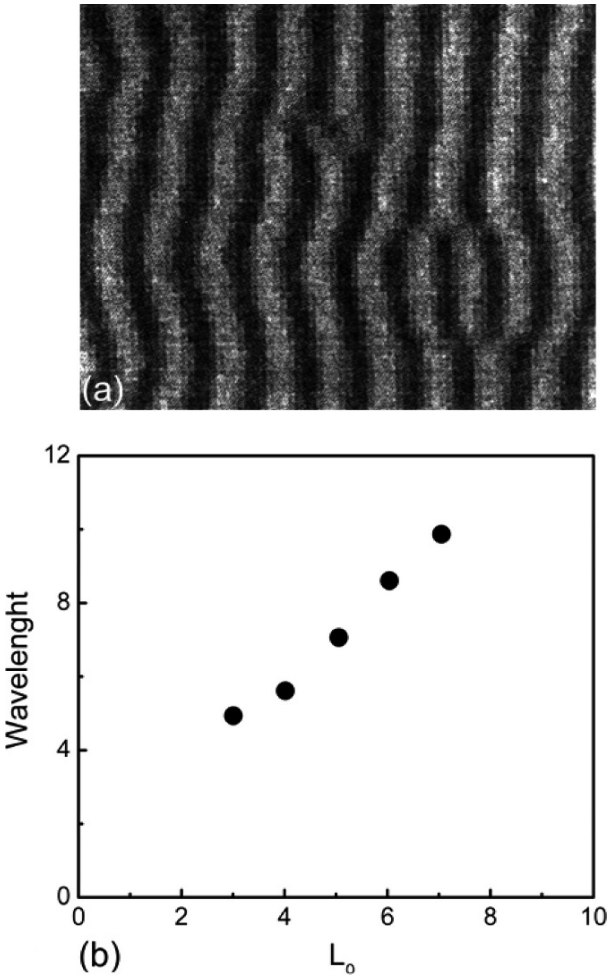

Fig. 6.15. (a) The asymmetrical shape of aeolian sand ripples simulated by Nishimori-Ouchi model, and **(b)** the influence of L_0 to wavelength (from Nishimori and Ouchi 1993)

models are generally given by simplifying the actual physical process, so it can not reflect the physical mechanism of sand movement in formation of aeolian sand ripples objectively and comprehensively. In addition, the simulation results are very difficult to correspond with the real time scale which also makes their simulation results do not agree with the actual aeolian sand ripples in quantity, and not be unable to effectively forecast the entire evolution process of aeolian sand ripples, i.e. the coarsening, the merge and the saturation of aeolian sand ripples. Besides, it is unable to effectively investigate the influences of wind velocity and sand particle size to the formation and evolution of aeolian sand ripples with these models, which makes them impossible to forecast the threshold wind velocity and the development of the Y-junctions in three-dimensional space, such as the change of the number of Y-junctions with wind velocity, time and particle diameter, and the migration of Y-junctions mentioned in Sect. 6.1.1.

6. 4. Discrete Particle Tracing Method (DPTM) Model

6.4.1 Basic Method

In this model, three main factors relevant to the formation of the aeolian sand ripples are considered. They are the wind-blown sand flux above the sand bed formed by sand particles with different diameters, the particle-bed collision and the rebound and ejection of sand particles after collision, as well as the saltation of high-speed sand and the creep of low-speed sand (transportation and deposition of creeping sand), respectively. The model main simulation steps are as follows:

Step 1: Establishment of initial sand bed which is similar with actual natural sand bed surface. This model is different from the Cellular Automaton model and the Coupled Mapping Lattice model, but is the same as the Discrete Element model, namely, the basic task of this model is to trace the motion of sand particles in the sand bed. The simulation sand bed is generated by the cooling method (see in Sec 3.5.1). It is composed of three particle sizes: fine (0.2 mm), middle (0.3 mm) and coarse (0.4 mm) with a ratio of 2:5:3. It is about 60 cm in length and 1.5 cm in width. Particle size is chosen statistically from lognormal distribution which is the same as natural sand particle distribution.

Step 2: Taking the time step as 1 s, the model uses the statistical coupled model (see in Sect. 5.2.1) to calculate the steady wind-blown sand flux. It can obtain the particle concentration and the distribution of sand particles' velocities changing with height above the sand bed under a given friction wind velocity, and further the number of incident sand particles and their

incident velocities and angles. Based on the concentration of sand particles and the distribution of sand particles' velocities per height cell, the incident sand particles will be inputted into the simulation system from the left boundary according to certain spacing and time interval. Here, periodic boundary is employed, namely, if the reptating sand departs from the right boundary, then it renters into the computation region again from the left boundary.

Step 3: Distinguishing the reptation and creep of bed surface sand according to the soft-sphere collision model (see in Sect. 3.3.2). Since the sands taking part in the formation of aeolian sand ripples are mainly composed of the reptating sands ejected from bed surface, so after obtaining the impacting speed and angle of saltating sands, we adopt the soft-sphere collision model to determine the number, position, speed and angle of ejected sands, then discriminate the type of sand movement (creep or reptation) according to the vertical speed of ejected sand.

Step 4: Determining the transportation and deposition of reptating sands according the movement of reptating sands. For the reptating sands, their trajectories can be calculated by solving saltation trajectory Eq. 5.12. Then, we compute the local wind field around aeolian sand ripples so as to introduce the influence of bed fluctuation on the local wind field and further on the formation of aeolian sand ripples. The creeping sands particles can't fly away from the sand bed but only roll over the other sand particles on the bed. Therefore, these particles lose their energies and finally stop due to friction work, and their final settling positions are determined by considering the friction and gravity during their creeping. Assuming a creeping sand particle rolls over another n sand particles to stop on bed surface, in which n_1 sand particles belong to the stoss slope α_{ss}, n_2 particles belong to the lee slope (angle of lee slope α_{ls}), this process satisfies the follow inequation:

$$0 \le W_s + W_g + nW_f < m_s g D_s \left(1 + \frac{\mu}{4}\right), \tag{6.8}$$

where, the kinetic energy W_s, the gravity work W_g and friction work W_f of the creeping sand particle can be respectively expressed as follow:

$$W_s = \frac{m_s}{2}\left[\dot{x}^2 + \dot{z}^2\right],$$

$$W_g = -n_1 D_s \sin\alpha_{ss} + n_2 D_s \sin\alpha_{ls},$$

$$W_f = -\int_{-\pi/6}^{\pi/6} m_s g\mu \frac{D_s}{2}\cos\theta_c d\theta_c = -\frac{1}{2} m_s g\mu D_s \ .$$

θ_c is the angle between the line connecting the centroid of two contacting particles and perpendicular.

Step 5: Determining the computational time steps according to the pattern of bed surface. After all saltating sands entered into the system, and all reptating sands completed their movements (maybe more than once), we define one computational time step is completed. If the scale of aeolian sand ripple obtained in this time step is the same with that in the previous time step, which means the aeolian sand ripple achieves saturation, then stop inputting sands into the system, and the simulation is end. Otherwise return to the step 2, and carry on the next computation step, the bed surface obtained in this step serves as the initial bed surface for the next computional time step.

Obviously, the difference between the discrete particle tracing method (DPTM) and the above models is that the DPTM traces the reptation and creeping motion of every ejected sand particle, which reflects the discreteness of wind-blown sand system. At the same time, through computing the wind-blown sand flux, the local wind field around aeolian sand ripples and the particle-bed collision process, it can reflect the interaction between wind field and sand movement and the integral behavior of wind-blown sand movement. Besides, the operation step in this model is taken as the real time (for example, in Zheng et al. (2008), the time step was taken as 1s, which can be further subdivided or extended according to the required precision), so it can realize the time correspondence between the simulation results and the actual states, furthermore it can realize the reproduce the formation and evolution of natural aeolian sand ripples, and obtain the threshold time when the aeolian sand ripples reaching saturation.

6.4.2 Major Simulation Results

The discrete particle tracing method (DPTM) is not only able to simulate the basic shape and the characteristic of an aeolian sand ripple in the 'mixed' sand case, such as particle size segregation of ripple, but also to reproduce the development process of aeolian sand ripples from unsaturation to saturation. In addition, it can predict the propagation velocities of the saturated aeolian sand ripples, the influence of wind velocity and diameter to the scale and saturation time, and the threshold wind velocity when ripple appear and disappear (Werner et al. 1986). Fig. 6.16 is the pattern of a simulated aeolian sand ripple, and the shape is asymmetric,

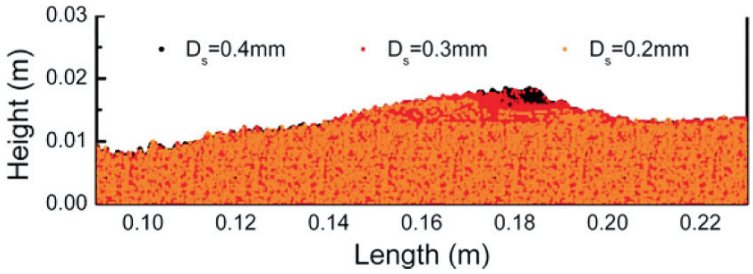

Fig. 6.16. The aeolian sand ripple in 'mixed' sand case simulated by the DPTM, the incoming friction wind velocity is taken as 0.5 $m \cdot s^{-1}$, the sand bed is composed of three particle sizes, fine (0.2 mm), middle (0.3 mm) and coarse (0.4 mm) with a ratio of 2:5:3, which is 60 cm in length and 1.5 cm in height including about 10^5 sand particles (from Zheng et al. 2008)

Table 6.1. Simulated results (u_*= 0.5 $m \cdot s^{-1}$) and experimental results (from Zheng et al. 2008)

Particle diameter [mm]	λ [cm]	H [cm]	RI	α_{ss}	α_{ls}
0.3 (with creep)	12.62	0.715	17.65	9°	17.32°
'Mixed' sands (with creep)	11.52	0.54	21	7.3°	19.3°
0.3 (without creep)	12.05	0.5	24.1	8.44°	8°
'Mixed' sands (without creep)	9.7	0.4	24.25	7.8°	11°
Experiments	7–14	0.5–1.0	15–20	8°–10°	20°–30°

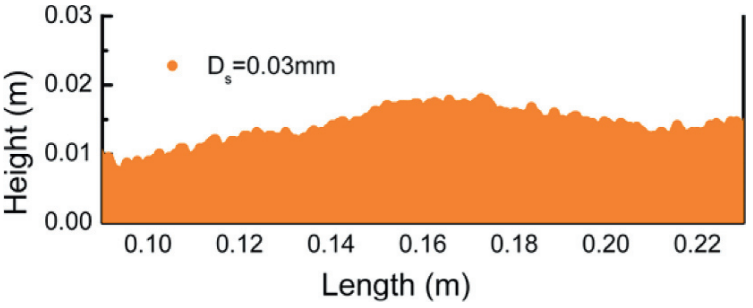

Fig. 6.17. The aeolian sand ripple in the 'uniform' sand case without considering the creeping sand, friction wind velocity is 0.5 $m \cdot s^{-1}$, sand diameter is 0.3 mm, the sand bed is 60 cm in length and 1.5 cm in height including about 10^5 sand particles (from Zheng et al. 2008)

with convex upwind (stoss) slopes, and concave lee slopes, which agree with experimental observation result of Anderson and Bunas (1993) as well as Werner et al. (1986) etc. (see Table 6.1 for comparisons in detail). Moreover, it can also present the stratification structure, that is, coarse particles are accumulated on the crest, and fine particles are in the trough of the ripple. At the same time, the simulation results also demonstrate that if the influence of

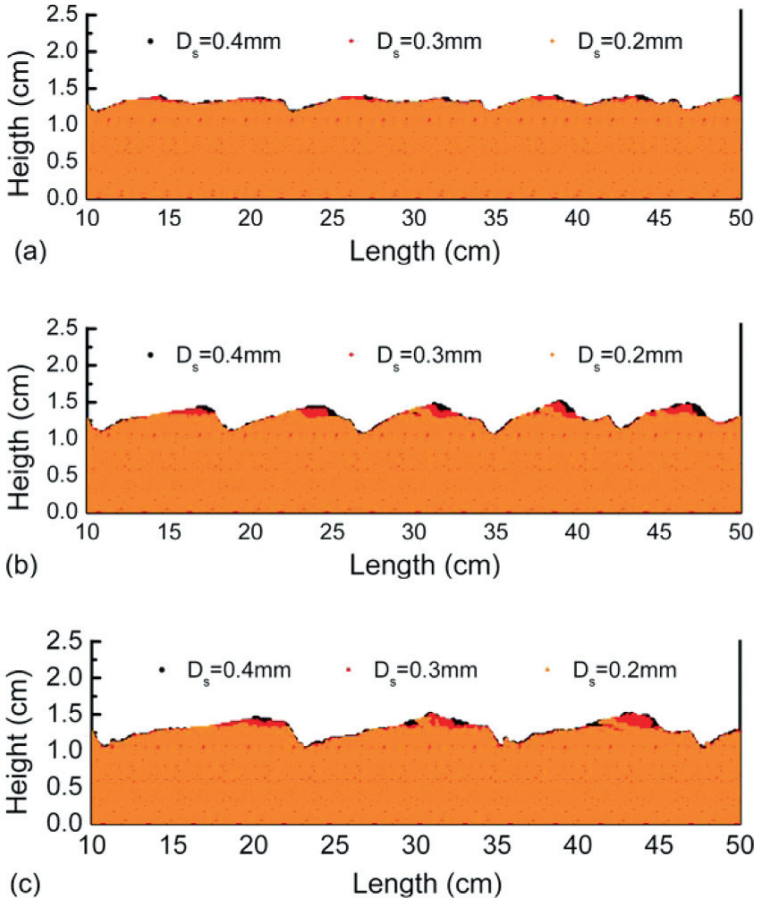

Fig. 6.18. Evolution of aeolian sand ripples: **(a)** tiny structure at t = 80 s, **(b)** mergence of tiny structure at t = 180 s and **(c)** saturated aeolian sand ripples at t = 440 s; the friction wind velocity is taken as 0.5 m·s^{-1}; the sand bed is composed of three particle sizes, fine (0.2 mm), middle (0.3 mm) and coarse (0.4 mm) with a ratio of 2:5:3, which is 60 cm in length and 1.5 cm in height including about 10^5 sand particles (from Zheng et al. 2008)

the surface creeping is not considered in the 'uniform' sand case, the surface of the simulated aeolian sand ripples are rough and symmetrical in shape (see Fig. 6.17) and the wavelength is clearly smaller than the real one. It indicates that it is necessary to consider the surface creeping in the simulation of the aeolian sand ripples.

The simulated results can also replay the formation process of aeolian sand ripples, that is, the initial flat sand bed starts deforming and tiny structures are observed (see Fig. 6.18a), and then these tiny structures started merging so that the pattern exhibits coarsening (see Fig. 6.18b), and finally the pattern tends to be saturated (see Fig. 6.18c). This is completely consistent with the results of field observations and wind-tunnel experiments. It is worth pointing out: the saturation time in the 'mixed' sand case is shorter than that in the 'uniform' sand case. The simulations also show that: the scale of saturated sand ripple is related with the incoming friction wind velocity and sand diameter (see Fig. 6.19). During the formation and evolution of sand ripple, it always moves forward along wind direction associated with the increase of ripple scale before achieving saturation, after that, the sand ripple maintains its shape and scale moving along wind direction. In addition, the migration velocity of saturated ripple is also related with the incoming shear wind velocity and sand diameter, for

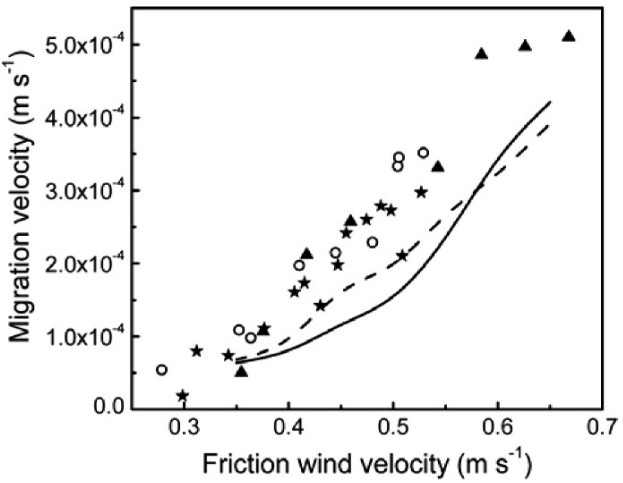

Fig. 6.19. The variations of propagation velocities of aeolian sand ripples with wind velocity. ★ measured results of field observation by Andreotti et al. (2006); ○ measured results in the Badain Jaran Desert by the author et al.; ▲ measured results in the multi-function environmental wind tunnel of Lanzhou University by the author et al.; ——— and – – – – represent the simulated results by the DPTM (Zheng et al. 2008) in the 'uniform' sand and the 'mixed' sand cases, respectively

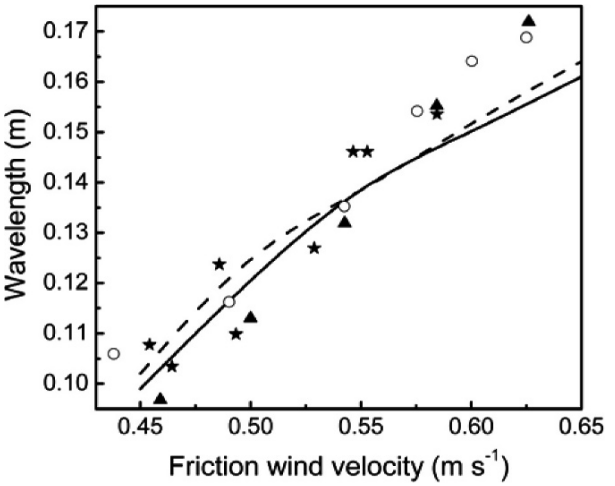

Fig. 6.20. The variations of the wavelengths of aeolian sand ripples with friction wind velocity. ★ measured results of field observation by Andreotti et al. (2006); ○ measured results in the Badain Jaran Desert by the author et al.; ▲ measured results in the multi-function environmental wind tunnel of Lanzhou University by the author et al.; ——— and – – – – represent the simulated results by the DPTM (Zheng et al. 2008) in the 'uniform' sand and the 'mixed' sand cases, respectively

example, the migration velocity increases with friction wind velocity increasing (see Fig 6.20). When the friction wind velocity is 0.5 $m{\cdot}s^{-1}$, the migration velocities of the saturated aeolian sand ripples are 1.454×10^{-4} $m{\cdot}s^{-1}$ and 1.885×10^{-4} $m{\cdot}s^{-1}$, respectively for the 'uniform' sand case (0.3 mm) and the 'mixed' sand case, which agree with the observed value (2.586×10^{-4} $m{\cdot}s^{-1}$) in the wind tunnel experiment (Bagnold 1941) in magnitude. Moreover, we obtain the threshold friction wind velocity for the appearance and disappearance of the aeolian sand ripples with our simulations. For both the 'mixed' sand case and the 'uniform' sand case (D_s = 0.3 mm), the threshold friction wind velocities are 0.3 $m{\cdot}s^{-1}$ and 0.7 $m{\cdot}s^{-1}$, which means that when the friction wind velocity is less than 0.3 $m{\cdot}s^{-1}$, the wind field is too weak to form aeolian sand ripples. However, when the wind velocity is larger than 0.7 $m{\cdot}s^{-1}$, the deposition of sand becomes so difficult that the wind ripples can not be formed.

Extending this model to simulate sand ripples in three dimensional space (1.6 m×1.2 m), it can reproduce the formation of the Y-junctions and their development process. From Fig. 6.21a, we can see that in the initial stage, the length of the crest-line of aeolian sand ripples are short and different everywhere. During the merging stage, these ripples interconnect each other forming many Y-junctions (see Fig. 6.22a). Afterwards, during

the development stage from unsaturation to saturation, as the ripples moving forward, the Y-junctions are gradually separated from the upwind ripples, and connected with the downwind ones. This kind of migration of Y-junctions to a certain extent promotes the enlargement of the aeolian sand

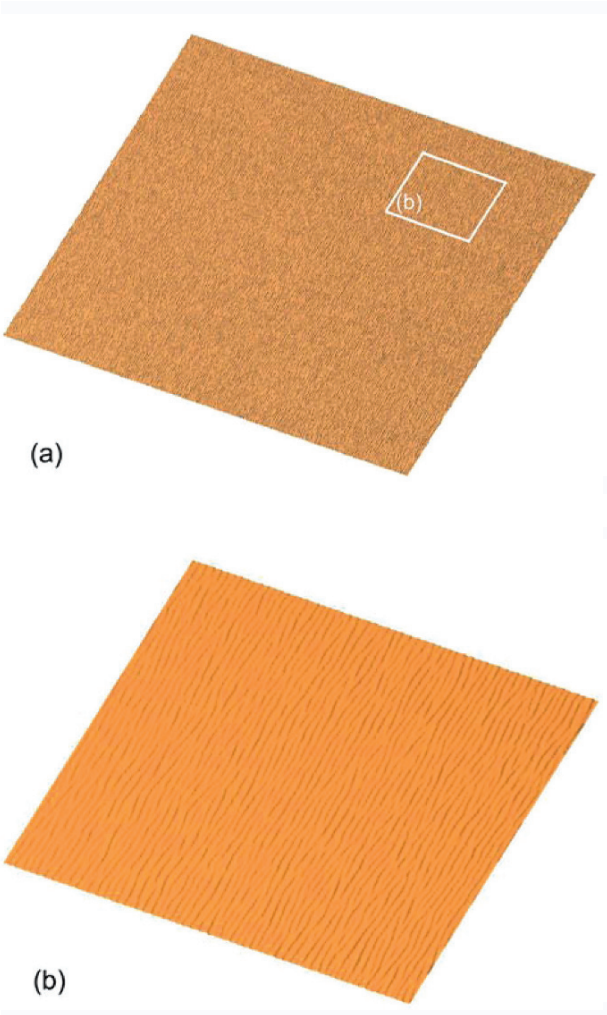

Fig. 6.21. The formation and evolution of Y-junctions simulated by the DPTM, **(a)** The tiny structures occur on bed surface at $t=22$ s; **(b)** locally enlarged drawing of a part of bed surface of (a); the sand diameter is 0.3 mm; the simulation area is 1.2 m×1.2 m, the depth of the sand bed is 2 cm, which includes about 2.5×10^7 particles (by the author et al.)

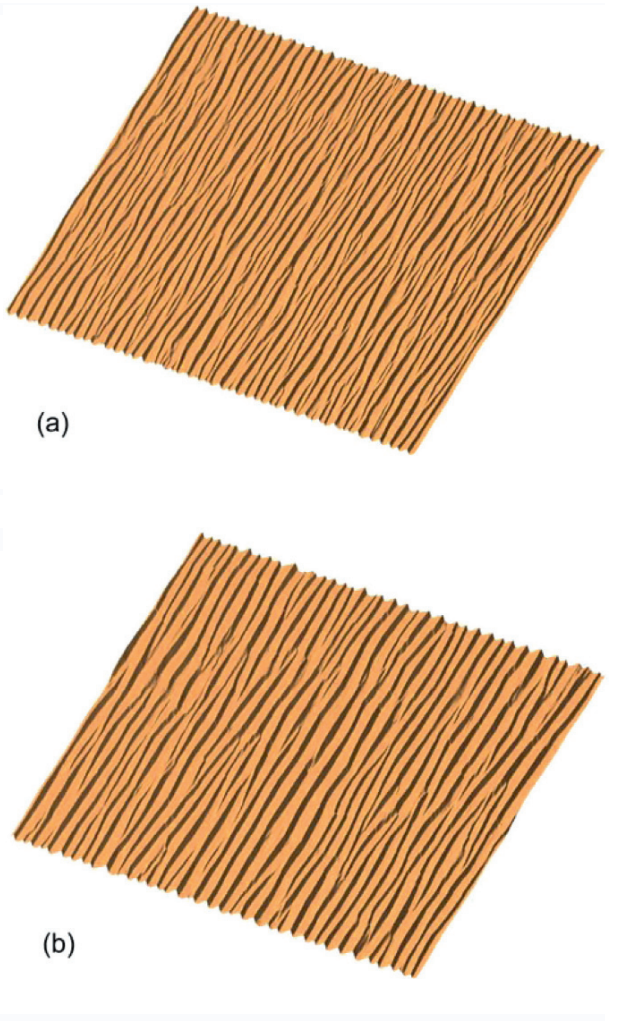

Fig. 6.22. The formation and evolution of Y-junctions simulated by the DPTM, **(a)** tiny structures start merging at t=268 s; **(b)** the aeolian sand ripples are mature (saturated) at t=536 s; the friction wind velocity is 0.5 $m \cdot s^{-1}$; the sand diameter is 0.3 mm; the simulation area is 1.2 m×1.2 m, the depth of the sand bed is 2 cm, which includes about 2.5×10^7 particles (by the author et al.)

ripple's scale. However, when the sand ripples are saturated, the number of Y-junctions obviously decreases (see Fig. 6.22b). From our simulations, we found that the wavelength of upwind junction is less than that of downwind, and their difference firstly decreases and then increases with the friction wind velocity (shown in Fig.6.23), which agree with the results given

by field observations (shown in Fig.6.5). Besides, our simulation results also reveal that the number of Y-junctions decreases with incoming friction wind velocity increasing.

If we efface a part of the saturated sand ripple in three dimensional space (see Fig. 6.24a), then new sand ripples will reappear in the effaced area under the action of wind field in our simulation (see Fig. 6.24b). After that, these new ripples will gradually connect with their neighboring undestroyed ripples until reaching saturation (see Fig. 6.25a). The initially destroyed traces are eliminated so completely that it seems the same as the state before effacement. However, comparing the same region with and without effacement (see Fig. 6.25b), we find the number of Y-junctions in creases after self-reparation.

The difference between the discrete particle tracing method and the continuous models is that the former reflects the discreteness of sand particles; it connects the reptation of sand particles with wind velocity and sand diameter through the particle-bed collision model, the trajectory equation of saltating sand and the computation of surface creeping. The main physical processes of wind-blown sand movement can be described by the existing

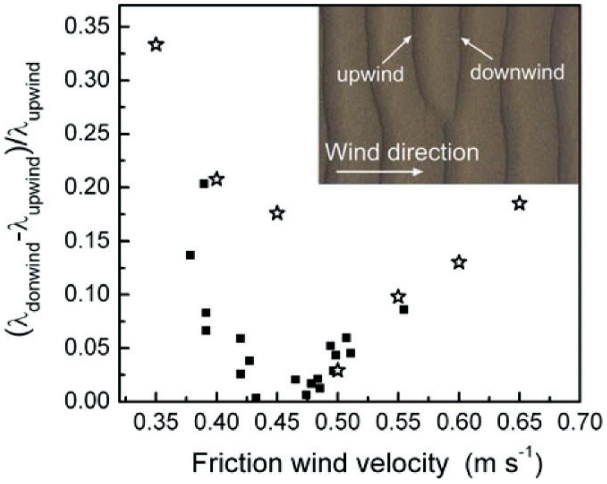

Fig. 6.23. The difference between the downwind wavelength ($\lambda_{downwind}$) and the upwind wavelength (λ_{upwind}) of Y-junctions for different friction wind velocities. ☆ – the simulated results by the DPTM (the friction wind velocity is 0.5 m·s^{-1}; the sand diameter is 0.3 mm; the simulation area is 1.2 m×1.2 m, the depth of the sand bed is 2 cm, which includes about 2.5×107 particles); ■ – measured results in the Badain Jaran Desert, the embedded picture is a photo of a Y-junction captured by the author et al. in the Desert

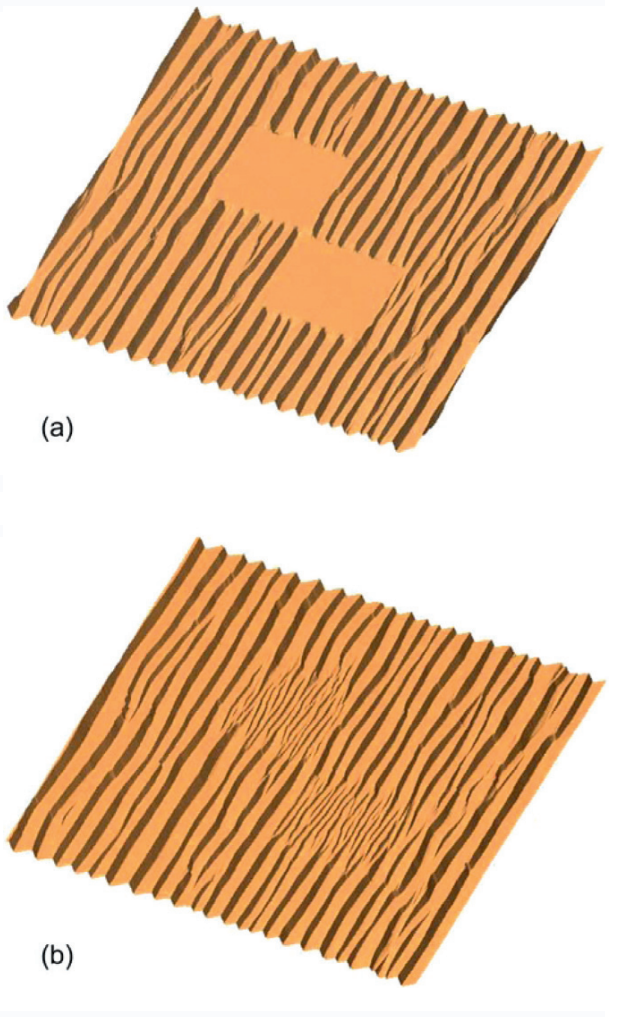

Fig. 6.24. The self-reparation behavior of aeolian sand ripples simulated by the author et al. (the friction wind velocity is 0.5 m·s^{-1}; the sand diameter is 0.3 mm; the simulation area is 1.2 m×1.2 m, the depth of the sand bed is 2 cm, which includes about 2.5×10^7 particles): **(a)** parts of the ripple surface are effaced; **(b)** new ripples appear in the effaced area with tiny Y-junctions at t = 54 s; (by the author et al.)

theoretical model in the DPTM without introducing new model parameters. Compared with the existing discrete model, the treatment of ejection, transportation and deposition in the DPTM is more close to the actual state, such as the impacting speed and angle of saltating, the position and

speed of ejected sand, and the calculation of the reptation particles through considering friction force etc. Moreover, the scales and propagation velocities of aeolian sand ripples obtained by the DPTM agree well with the actual values in quantity. Besides, it can reproduce the developing process of

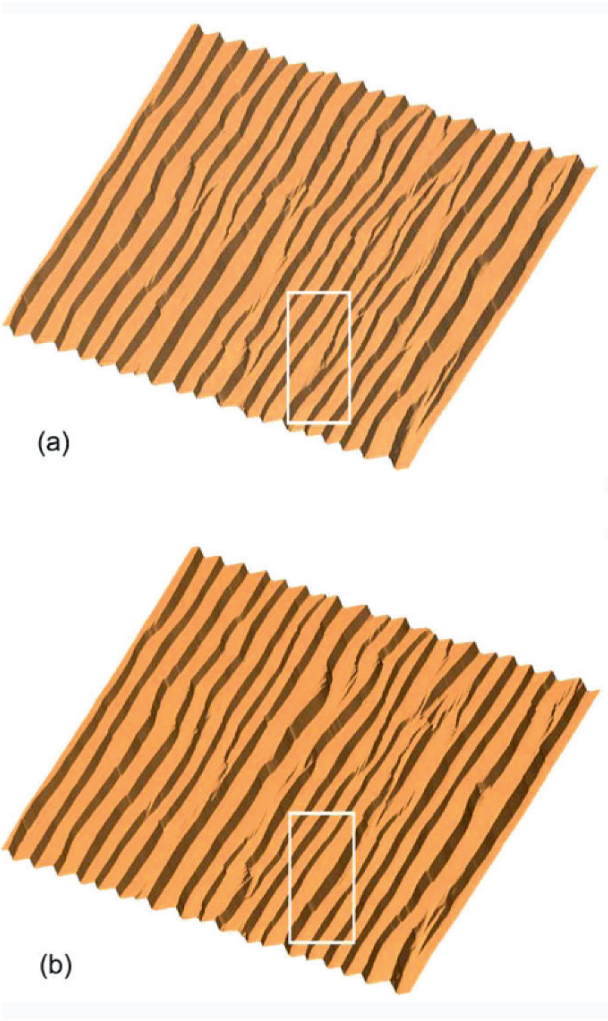

Fig. 6.25. The self-reparation behavior of sand ripples simulated by the author et al. (the friction wind velocity is 0.5 m·s^{-1}; the sand diameter is 0.3 mm; the simulation area is 1.2 m×1.2 m, the depth of the sand bed is 2 cm, which includes about 2.5×10^7 particles): **(a)** the configuration of the bed surface at $t = 220$ s, with new junctions appearing compared with **(b)** the configuration of the bed surface without effacement at $t = 220$ s in the same area (by the author et al.)

aeolian sand ripples, and predict the influence of wind velocity and diameter to the scale and saturation time of an aeolian sand ripple, as well as the threshold wind velocity for appearance and disappearance of an aeolian sand ripple.